Geopersia 2024, 14(2): 291-306
DOI: 10.22059/GEOPE.2024.370003.648740

RESEARCH PAPER

Endorsing Trusheim's classic model of salt-diapir growth by the interpretation and restoration of seismic lines in the southern region of the Great-Tunb Island, Persian Gulf

Mehrsa Haji Khani [1, *], Mahdi Najafi [2], Seyedmohsen Seyedali [3]

[1] Department of Earth Sciences, Institute for Advanced Studies in Basic Sciences (IASBS), Zanjan, Iran
[2] Geosciences Barcelona, Geo3Bcn-CSIC, Lluís Solé i Sabarís s/n, 08028 Barcelona, Spain
[3] Department of Geophysics, Iranian Offshore Oil Company (Falat-Ghare), Tehran, Iran

Received: 22 December 2023, Revised: 05 April 2024, Accepted: 29 April 2024

Abstract
This paper investigates the geometry and evolution of the Oligocene and lower Miocene Fars salt diapirs and adjacent minibasins in the southeast Persian Gulf. Utilizing 2D offshore seismic lines, integrated with well data, we conducted detailed interpretations to construct NE-trending geological cross-sections south of the Great-Tunb Island. Subsequent stepwise restoration, guided by thickness patterns of syn-kinematic sediments, local unconformities, growth strata, and halokinetic sequences, unveiled the growth history of salt massifs, turtle anticlines, and salt horns featuring normal fault systems at their crests. Our findings reveal a synchronous evolution of Fars salt diapirs and nearby minibasins, aligning significantly with the classic (Trusheim, 1960) concept. The identified stages encompass; 1) The pre-kinematic stage, coinciding with the deposition of the Gachsaran Formation in the Lower and Middle Miocene; 2) the Growth of salt pillows, concurrent with the basal deposition of the Guri Member at the Middle and Late Miocene boundary; 3) Passive and rapid diapir growth, synchronous with the Guri Member deposition in the Late Miocene; and 4) The post-diapirism stage and basins associated with salt incompressibility, corresponding to the deposition of the Upper Mishan and Aghajari formations during the Late Miocene and Pliocene times.

Keywords: Salt Diapirism, Marine Seismic Data, Kinematic Evolution, Minibasin, Fars Salt, Hormuz Salt.

Introduction

The evolution of salt diapirs and surrounding minibasins has always been an intriguing subject for geoscientists. The primary interest in salt diapirism stems from the oil and gas industries, as many of the world's major hydrocarbon provinces are located in salt basins, including the Persian Gulf, Caspian Basin, Gulf of Mexico, North Sea, Congo Basin, and Campos Basin (Jackson & Hudec, 2017).

The pioneering works by (Trusheim, 1957, 1960), a German geologist known as the father of modern salt tectonics, proposed a diapiric evolution model known as 'Trusheim's classic model.' In this model, four evolutionary stages of salt movement have been proposed: 1) Pre-kinematic stage: The constant thickness sedimentation occurs before the beginning of any deformation in the basin (Fig. 1a). 2) Pillow Stage: It involves free subsidence into the salt and is named the "pillow stage," where a salt pillow starts to grow, and the central part of the minibasin is the thickest. The beginning of the salt withdrawal is transferred from the Middle

* Corresponding author e-mail: mehr.7522@gmail.com

of the minibasin to the core of the pillow. The depocenter is located in the Middle of the basin (Fig. 1b). 3) Diapir Stage: The rising salt pierces the overburden. The center of the depocenter no longer subsides, and salt is evacuated from the minibasin flanks. The salt pillow is converted to a diapir in this stage, and the basal weld extends laterally. The depocenter moves towards the margin, and during this stage, an erosion surface is created between the syn-diapir sedimentary sequence and the syn-pillow sedimentary sequence (Fig. 1c). This stage involves the gradual withdrawal of salt from minibasin flanks and the movement of the weld towards the surroundings. The welding pinches off, resembling a zipper, causing the depocenter position to change, and the thickness of sediments increases as they approach salt structures. 4) Post-Diapir Stage: The salt rise reaches its maximum, and there are some changes in thickness because of different compaction between salt and surrounding strata (Fig. 1d). The minibasin can no longer subside because all points of the diapir have pinched off, and the entire salt layer has been evacuated. Under the overburden pressure, water exits from the sediment pores, and sediments undergo compaction after diagenesis. Evaporitic sediments, such as mudstone and sandstone, experience higher compaction compared to salt. This is because salt, having no grains, is compacted to a lesser extent than sediments. As a result, a convex area occurs in post-diapir layers due to the compressibility difference (Fig. 1d). Eventually, the minibasin infill completely pinches, and no salt enters the salt wall (Peel, 2014). Following (Trusheim, 1957, 1960), further modifications were recommended to his model by (Vendeville, 2002), suggesting that, in general, extension forms salt pillows in which the roof of the pillow-like structure is formed by early normal faulting.

In this paper, we focus on a case study of the Great-Tunb Island, located in the southeast Persian Gulf offshore Iran. In the Persian Gulf, the most well-known diapirism is associated with Hormuz salt dating back to the Ediacaran/Early Cambrian period (Callot et al., 2012; Jahani et al., 2007; Kent, 1979; Ala, 1974; Stewart, 2018). Recent studies have introduced Oligocene Fars salt diapirism in the southeastern part of the Persian Gulf (Jahani et al., 2007; Ezati et al., 2019; Faghih et al., 2019; Hassanpour et al., 2021; Snideo, 2020) (Fig. 2).

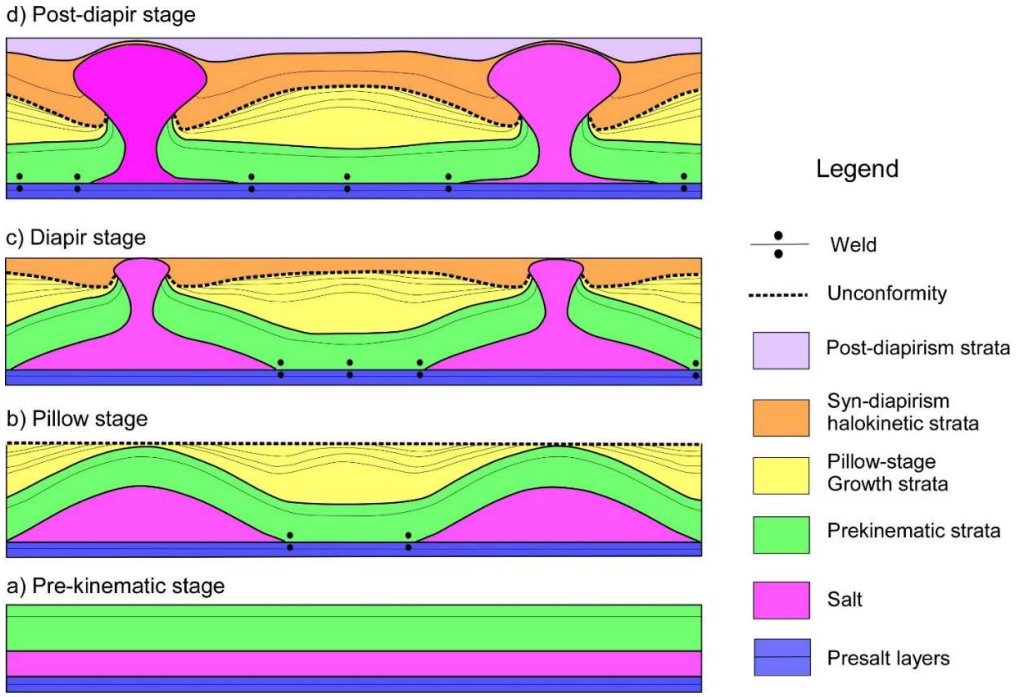

Figure 1. Lateral subsidence evolution during the growth of a salt pillow and diapir, illustrating four kinematic stages: pillow stage, diapir stage, and post-diapir stages. Adapted from salt diapirs of the northern German salt basin (Trusheim, 1957, 1960)

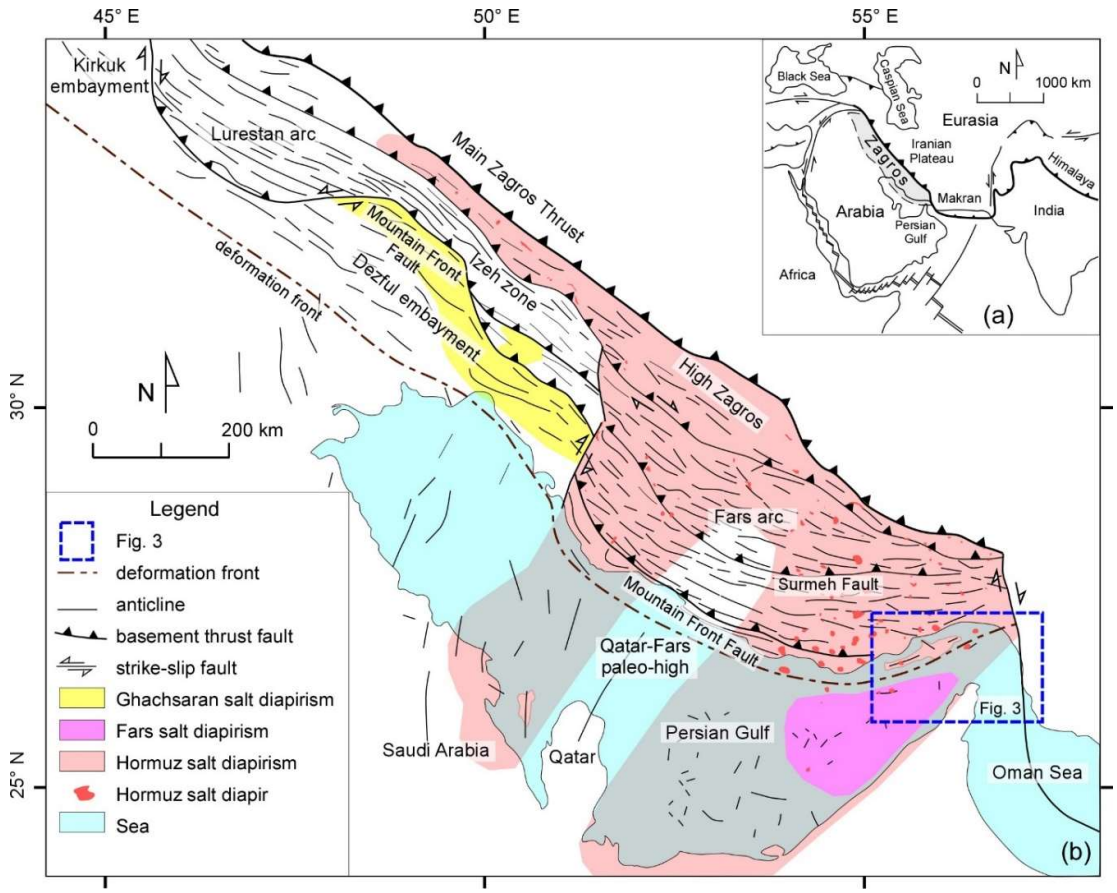

Figure 2. Geographic distribution map of three diapiric basins in the Zagros folded belt, adapted from (Najafi & Lajmorak, 2020). The blue rectangle highlights the location of the study area in the northeastern Persian Gulf

In the last five years, a considerable literature of several valuable studies has grown up around the Hormuz and Fars Salt diapirism due to the release of high-quality seismic lines in the southeastern Persian Gulf (Ezati Asl et al., 2019; Faghih et al., 2019; Hassanpour et al., 2020, 2021; Snidero et al., 2020).

(Faghih et al., 2019; Ezati Asl et al., 2019) performed two integrated studies on seismic lines around the Greater Tunb and Abu Musa islands, respectively. The spatial distribution of diapirs consists of a central and larger structure in these islands and the surrounding ring-like diapiric walls of the Fars Salt. These studies suggest 5–7-km-thick tabular- and wedge-shaped halokinetic sequences that infill minibasins and point to the downbuilding process during the deposition of the Gachsaran, Mishan, and Aghajari formations. However, (Ezati Asl et al., 2019) propose that the central diapir in the Greater Tunb Island is rooted in the Hormuz salt layer at the basement-cover interface and has been growing since Early Paleozoic times, soon after the deposition of the Hormuz salt.

(Hassanpour et al., 2020, 2021; Snidero et al., 2020) focus more on the kinematic interaction between the Hormuz and Fars salt systems in SE Persian Gulf, using seismic interpretation, sequential restoration, and physical modeling methods. These studies suggest that Hormuz diapirs rose passively during Paleozoic and Mesozoic times and were rejuvenated by contractional deformations during the Cenozoic. These studies infer that the diapirism of the Fars Salt layer was triggered by the kinematic interaction of the Hormuz salt system, in the Early Miocene. They suggest three mechanisms in which deeply-rooted overriding allochthonous Hormuz salt sheets trigger diapirism in the shallower Fars Salt layer. These

mechanisms differ depending on the assumed stratigraphic level of emplacement of allochthonous Hormuz salt sheets: a) (Hassanpour et al., 2020, 2021) show that contractional deformation related to the Oman orogenic system squeezed Hormuz diapirs and developed allochthonous salt wings and sheets at Palaeocene–Eocene levels. These studies suggest that the Fars Salt was more likely triggered by the loading of these salt sheets and wings underlying the Fars Salt as the evacuation or rearrangement of the salt within these sheets modified the geometry of the Fars Salt and triggered its lateral flow. (Snidero et al., 2020) studied the Tunb salt system and inferred that the emplacement of Hormuz Salt directly above the Fars Salt layer resulted in the interaction between the two salt units, and the development of wider salt inflation.

Despite all these different potential triggering mechanisms, the published studies agree that the development of Fars Salt structures has been driven mainly by differential sedimentary loading and downbuilding processes during the Neogene period. Although most previous studies show successful reconstructions from the Paleozoic to recent, the current study focuses on more detailed tectonostratigraphic patterns in Neogene minibasins. This allowed us to represent local but detailed steps of minibasin subsidence and diapir growth during the Neogene time.

The southeastern Persian Gulf is a region of great significance due to its rich oil and gas reservoirs. The study area in this paper is located in the southeastern Persian Gulf basin, specifically in the western strait of Hormuz, in the region south of Greater Tunb Island. This basin exhibits unique structural characteristics, marked by three factors of structural complexity: Hormuz salt structures, Fars salt structures, and deep faults around the strait of Hormuz. Notable islands in this area, including Qeshm, Greater Tunb, Lesser Tunb, Hormuz, Sirri, Hengam, Larak, and Abu Musa, are formed by Hormuz and Fars salt structures (Fig. 3).This study focuses on the Fars salt and the evolution of minibasins resulting from diapir growth in the south of Great-Tunb Island. The primary objectives are to determine the geometry of salt structures and the adjacent minibasins and to understand how salt structures evolved during geologic time through the analysis of syn-diapirism sedimentary patterns.

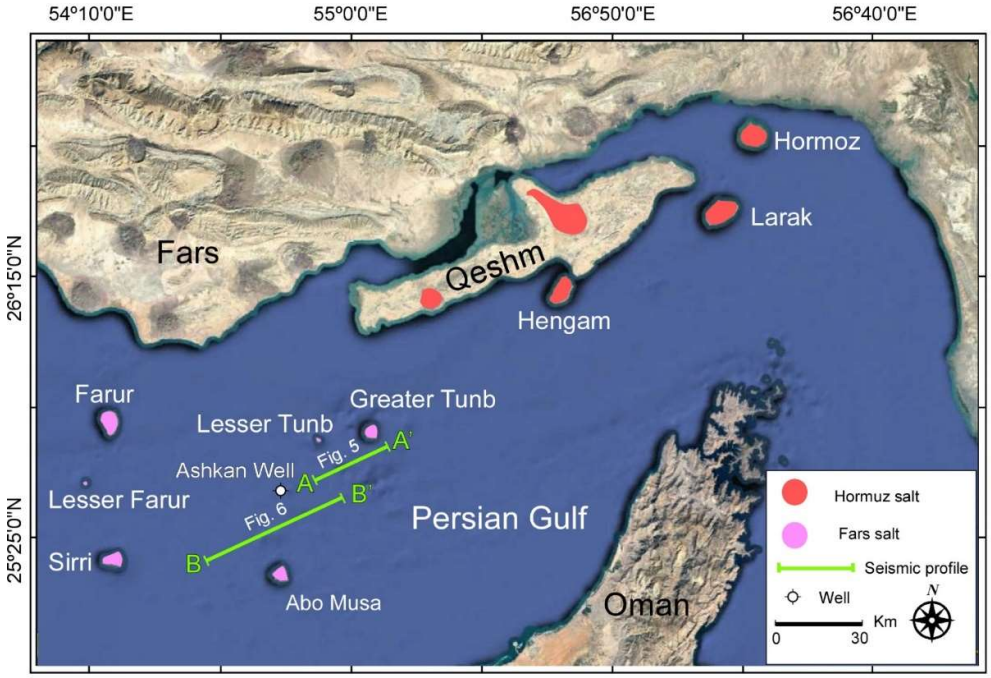

Figure 3. Study area in the southeastern Persian Gulf, indicating the location of islands and highlighting the individual positions of Hormuz and Fars salt diapirs

The methodology involved interpreting seismic lines in combination with drilled well tops. Subsequently, two structural cross-sections were constructed, followed by step-by-step restorations and the generation of kinematic evolution models of salt structures.

Cenozoic stratigraphy of the southeastern Persian Gulf

Fig. 4 demonstrates a simplified stratigraphy of the Cenozoic strata in the southeastern Persian Gulf. The lithostratigraphy of units is based on the Ashkan well data, and ages are determined according to (Pirouz et al., 2015; Najafi et al., 2021).

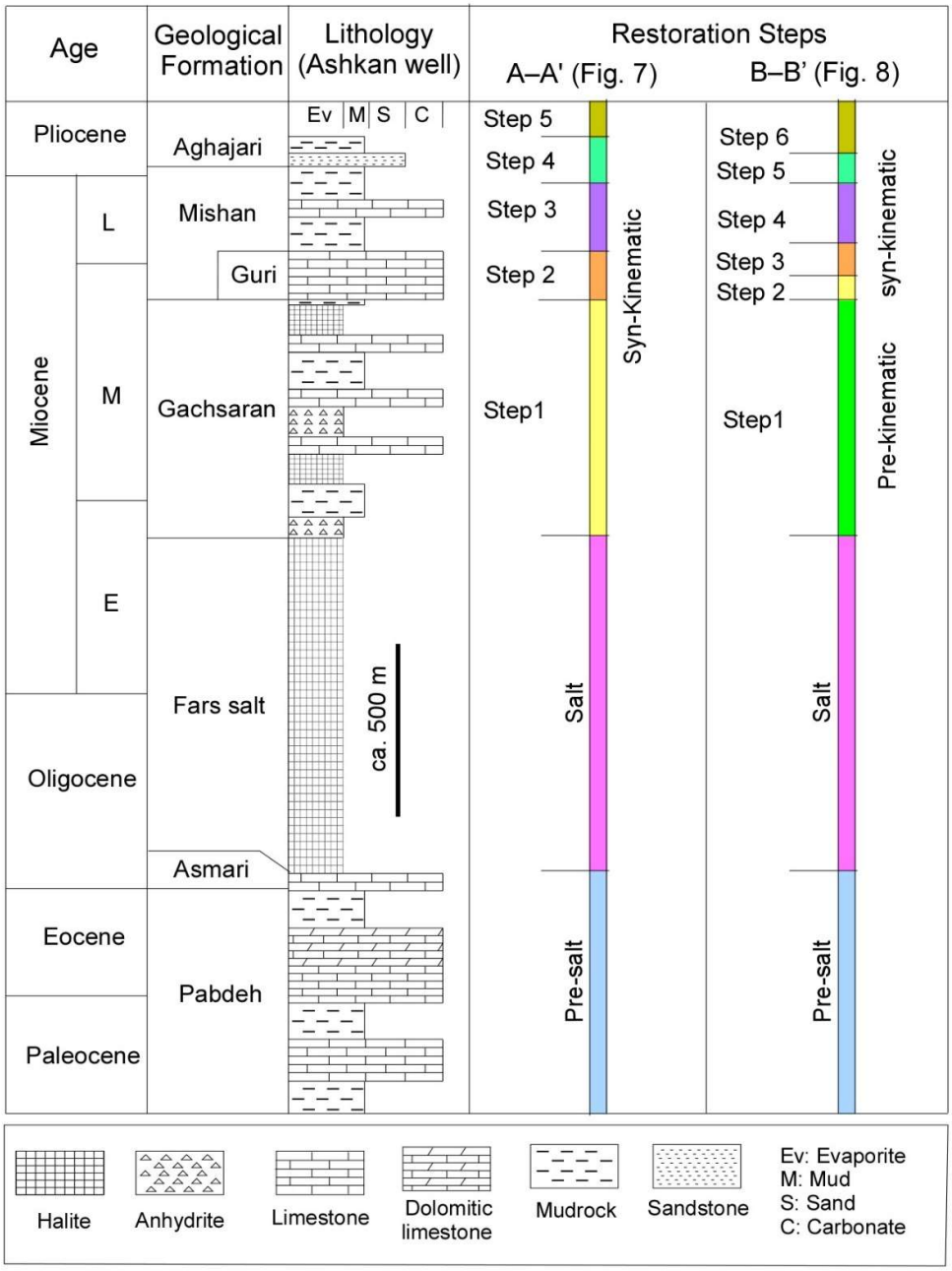

Figure 4. Stratigraphic column of the southeastern Persian Gulf based on Ashkan well data, shown in Fig. 2. The age of stratigraphic units is determined, and the evolutionary stages are plotted for seismic lines AA' and BB' (Pirouz et al., 2015; Snidero et al., 2020; Najafi et al., 2021)

Cenozoic stratigraphy of the study area, from old to young, is as follows. The Pabdeh Formation (Late Paleocene–Early Oligocene) is composed of approximately 620 m thickness resulting from the deposition of marl, limestone, and dolomitic limestone. The Asmari Formation (Oligocene–Early Miocene) comprises about 1040 m thickness, including limestone, oolite, and nummulitic limestone. In some regions of the Strait of Hormuz and the study area, limestones in the Upper sections of this formation are laterally replaced by Fars salt. The Gachsaran Formation (Early Miocene–Middle Miocene) is mainly composed of evaporites, marl, carbonates, and red shale with an approximate thickness of 645 m. The Mishan Formation (Middle Miocene–Early Pliocene) consists of marl and local limestones with an approximate thickness of 400 m. In this formation, the Guri Member is a sequence deposited under shallow-marine conditions and includes Miogypsina and Orbulina universa, representing the Middle Miocene age (Motiei, 1993). In the Upper-most part of the sedimentary succession, the Aghajari Formation is composed of a thick clastic sequence derived from the northeast orogenic source areas (Ghazabn, 2007).

Data and methodology

In this study, seismic and well data, along with related reports (Gazban, 2007; Alavi, 2004; Motiei, 1993), were gathered with the support of the Iranian Offshore (Falat-Ghare) Oil Company. The identification of top formations and seismic line sequences was accomplished through the analysis of formation tops in Ashkan well data. Subsequently, upon accurately identifying seismic lines, the sediments filling minibasins were categorized into several growth units based on unconformities and thickness variation patterns. Two balanced structural cross-sections, AA' and BB', after drawing in Petrel software, were drawn again in the Canvas program and finally restored step by step in Move software .At each restoration step, a chosen horizon was considered flat, and the remaining structures were adjusted to the same extent of retro deformation. The process involved identifying the target and old sedimentary horizons, followed by the restoration procedure. The horizontal target was progressively restored step by step, with the restoration steps constructed from older to younger in subsequent analyses.

Structural style

For the interpretation of seismic lines, sequences are divided into several units based on the thickness variation pattern of sediments, depocenter location, and unconformities. Subsequently, all stages are replicated according to this division. In this study, two balanced structural cross-sections are presented: AA’, approximately 40 km in length, extending from northwest to southeast with a depth of 3000 ms, and BB’, approximately 40 km in length, extending from northwest to southeast with a depth of 4000 ms (Figs. 5 and 6).

AA ’cross-section

Salt structure and fault geometries

The AA’s cross-section extends from northeast to southwest and encompasses two salt structures. Structure D1 is a cylindrical salt massif, measuring 1000 ms in height and 1010 m in length (Fig. 5). Salt migration has occurred from both sides of this structure. At the southwest of D1, a weld is observed between the suprasalt pre-kinematic horizon and pre-salt layers. The salt structure is truncated by several minor normal faults at the crestal domain (Fig. 5).

The salt structure D2 is a salt anticline with salt rising only from the northeastern part of the structure. This structure is truncated by later normal faults with a sub-vertical dip and a height

of 1000 ms, along with some secondary faults. Firstly, the sedimentary minibasin associated with D1 is examined and divided into A, B, C, and D based on the unconformity-bounded sequences with thickness variations. The depocenter in this sequence is variable and has migrated from the center toward D1 (Fig. 5). Subsequently, the mini-basins related to D2 are examined, which include three sequences B, C, and D, in which the depocenter has migrated towards D2.

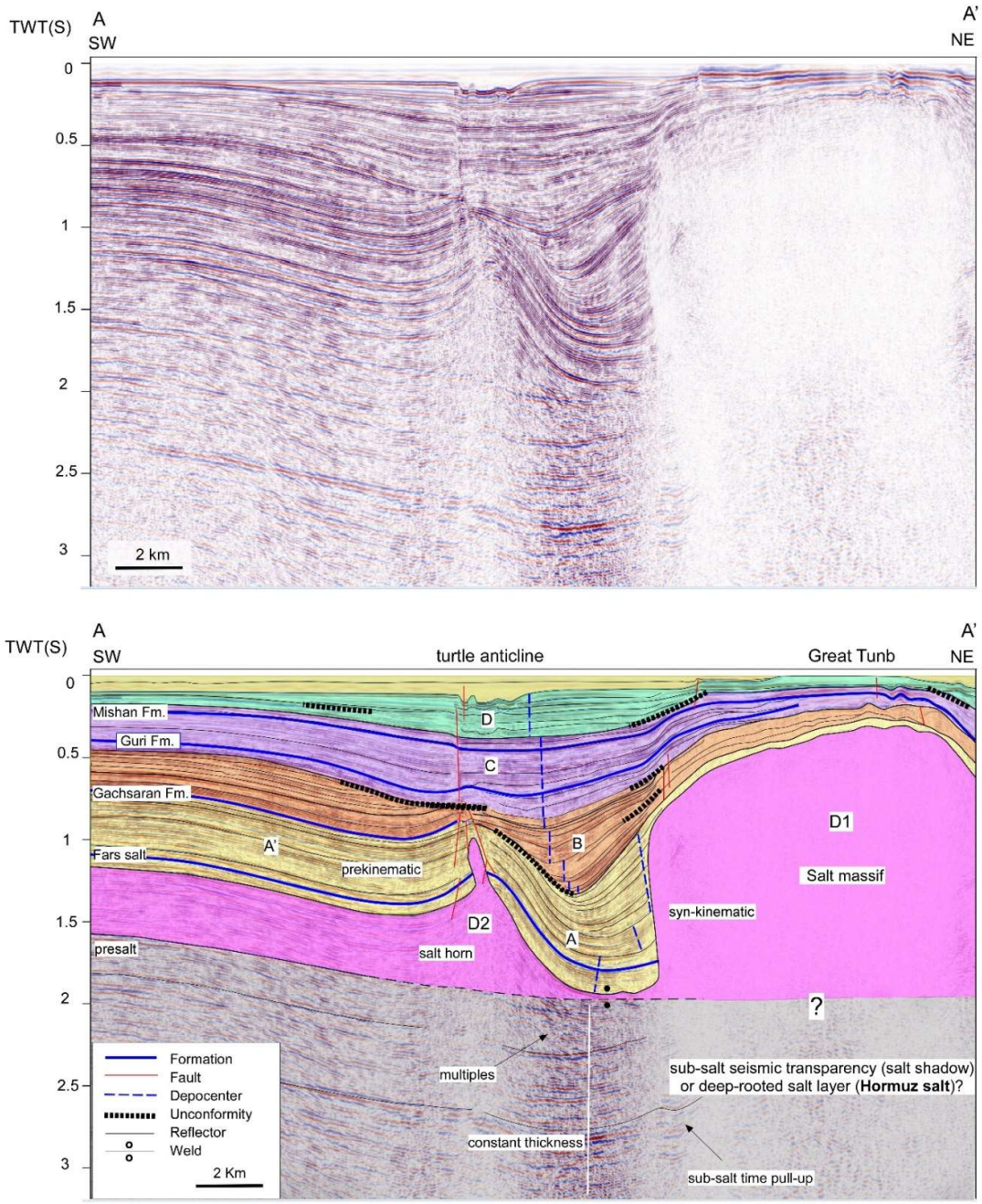

Figure 5. Two-dimensional seismic profile and structural cross-section AA' depicting the width of D1 salt massif and D2 salt anticline. The illustration includes surrounding minibasins, normal faulting, and the evolutionary stages of salt structures including pre-salt, salt-deposition stage pre-kinematic stage, pillow stage, diapir stage, and post-diapir stages. The Upper boundaries of the Fars salt (equivalent to the Asmari formation), Gachsaran Formation, Mishan Formation, and Guri Member are also indicated

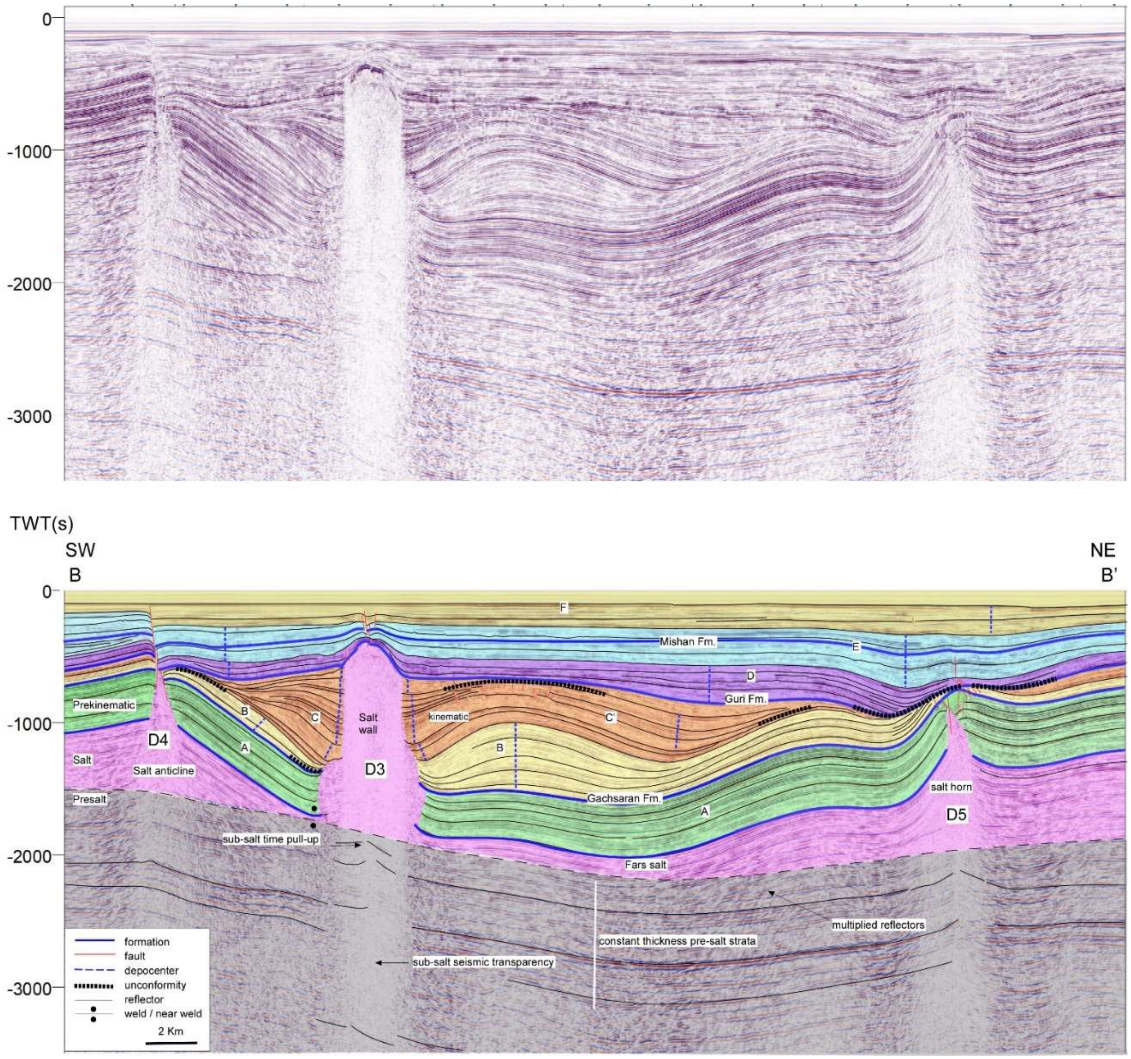

Figure 6. Two-dimensional seismic profile and structural cross-section BB', illustrating the D3, D4, and D5 diapiric structures. The visualization includes a salt stock diapir, universal welding in the bed of pre-kinematic sedimentary sequence, and normal faulting. Minibasins adjacent to diapirs showcases the evolutionary stages of salt structures including the pre-salt stage, salt stage, pre-kinematic stage, pillow stage, diapir stage, and post-diapir stages—with distinct colors

Thickness variation of sedimentary units in minibasins

At the base, the pre-salt sedimentary sequence maintains a constant thickness with salt covering it. Minibasins are situated around both salt structures, featuring a post-salt sedimentary sequence A of consistent thickness. Sedimentary sequences exhibit variable thicknesses between salt structures, with initial sediments deposited concurrently with the rise of salt (Fig. 5). From this perspective, the depocenter of this sequence is observed to migrate from the basin center toward the D1 diapir.

There is a weld between sedimentary sequence A and pre-salt sequences, along with a toplap between sequences A and B resulting from erosion. In sedimentary sequence B, the depocenter initially lies in the Middle of the basin, later migrating toward D2. An unconformity is evident between the sequences B and C. Thickness variation is notable in sedimentary sequences C and D, with the most significant thickness variation occurring over the two salt structures, named D1 and D2 diapirs (Fig. 5).

Minibasin geometry and interpretation

Based on the thickness variation of sediments in A, B, C, and D minibasins, the following evolutionary stages are interpreted (Fig. 5). The first stage predates salt structure growth, marked by initial sedimentation. In the second stage, the salt structure initiates growth concurrently with the deposition of the sedimentary sequence on its flanks. Sequence A illustrates the migration of the depocenter from the central zone toward the D1 diapir over time, indicating simultaneous salt withdrawal from beneath the sediments toward D1 during deposition (Fig. 5). The third stage witnesses the deposition of sequence B alongside the welding of sequence A, featuring a toplap between the two sequences. In sequence B, the depocenter migrates from the basin center toward the normal fault at the crest of the salt anticline, signifying the beginning of the growth of the D2diapir. An unconformity results from erosion in the fourth stage following the deposition of sediments in sequence B (Fig. 5). In the fifth stage, sediments are once again deposited on the top lap, creating sequence C, while the depocenter continues to migrate toward the normal fault. This indicates the ongoing growth of the D2 salt structure. During the sixth stage, the welding probably completes When the salt is completely drained from under the A mini-basin. The base of A mini-basin grounds on the top of pre-salt layers.(Fig. 5). In this stage, sediments undergo post-deposition vertical compaction. As salt lacks grains, it remains uncompacted, resulting in lower sediment thickness over the salt (Fig. 5).

BB's cross-section

Salt structure and fault geometries

The BB's cross-section, extending from northeast to southwest, encompasses three salt structures. Including a salt stock with a height of 1000 ms and a length of 250 m, a turtle anticline, featuring a near-vertical fault extending over 1000 ms, accompanied by some secondary faults at the crest of the D4 salt structure. Additionally, some normal faults are observed at the crest of the D3 salt structure. The A salt horn, standing at 450 m in height and 250 m in length is developed below the concentration of normal faults. Moreover, a few normal faults and local erosions are present at the crest of the D5 salt structure. Normal faults are also observed in the Upper region of the C minibasin (Fig. 6).

Thickness variation of sedimentary units in the minibasin

On both sides of the D3 diapir, there are sedimentary units with a variable thickness showing depocenter migrating toward the D3 diapir (Fig. 6). These units are examined individually. The sedimentary sequences, from older to younger, include pre-salt strata, and Fars salt, as well as pre-kinematic, kinematic, and overburden sediments. In the pre-salt sedimentary sequence, the thickness remains constant. The salt unit is positioned on this sedimentary sequence, giving rise to sequence A (Fig. 6). Welding occurs between the bed of sequence A and the pre-salt surface.

Sequence B exhibits variable thickness, with a minimal thickness in the southwest and a greater thickness between D4 and D5 diapirs. The depocenter of sequence B is located at the center of the basin. In sequence C, the thickness is also variable, and the depocenter progressively moves closer toward the D3 diapir over time. Additionally, a series of faults with top laps are observed at the bottom of sequence C. The thickness variation in sequence D is insignificant, thinning towards the crestal domain of the D3 diapir (Fig. 6). The depocenter of sequences E and F are also located at the basin center. In the northwestern parts of sequences E and F, the depocenter is situated at the crest of the D5 diapir. (Fig. 6).

Structural interpretation and evolution

Based on the thickness variation of sediments in minibasins and top laps mentioned above, the evolutionary stages are interpreted as follows: The first stage is related to the pre-kinematic or pre-growth of the D3 diapir. Then a series of syn-diapirism sequences are deposited above it (Fig. 6). In the second stage, the sedimentary unit B is first deposited in the southeast of D3, and an unconformity is observed at the base of the sequence B. However, the deposition in the Middle of sequence B is different from other sedimentary units. The depocenter is located at the basin center, which seems unrelated to salt structures in this seismic line. According to Trusheim's model, the depocenter is initially located at the basin's center and migrates to the flanks after the salt withdrawal from both sides (Fig. 6). Then, D3 starts growing simultaneously with the deposition process. As can be seen in sequence C, the depocenter continuously migrates toward D3 over time, showing that salt beneath the sediments has migrated toward D3 concurrently with the progressive deposition process (Fig. 6). The third stage is related to the growth of D3 simultaneously with progressive welding at the base of the sequence A. At the same time, in the northeast part of the cross-section, faulting has occurred, and D5 has started growing. In sequence D, the depocenter is almost in the Middle of the basin. In the fourth stage, concurrent with D5 growth, sequences E and F are deposited, in which, the thickness has increased at the crest of the D5 diapir (Fig. 6).

Step-by-step structural restoration

This study involves the step-by-step restoration of structural cross-sections (AA' and BB') to their pre-deformation stages (Figs. 7 and 8). Restoration refers to the re-establishment of the original geometry of sedimentary units before deformation, serving for validation and structural interpretation. Accurate and reliable data are crucial for proper restoration, such as seismic data aligning with well data in the study area (Groshong et al., 1999). A complete restoration requires meticulous consideration, avoiding overlaps, faults, layer bending, and non-horizontal layers.

For a correct restoration, attention must be given to the extent of deformation, fault block displacement, and internal deformation of fault blocks (Fossen, 2010). The restoration model in this study relies on two principles: the length conservation law for formations over time and the area conservation law for formations with ductile deformation including the Fars Salt layer. In this study, considering the extensive research on sediments and salt tectonics, five and six steps were respectively applied for the tectonic restoration of structural cross-sections (AA' and BB'). Each restoration step corresponds to a distinct deformational step. Sediments are categorized based on thickness variation patterns and unconformities, facilitating the presentation of cross-section evolution and restoration (Figs. 7 and 8). The restoration process proceeds step by step, moving from the present to the past. During each restoration step, the targeted horizon is flattened entirely, and other structures are adjusted accordingly by the retro-deformation algorithm.

Restoration results of AA's cross-section

The steps of structural evolution are elucidated in this section (Fig. 7). In the first step, a northeastern diapir forms the D1 diapir as a salt massif (Fig. 7-1). The boundary between the salt diapir and the surrounding sediments is an intersecting boundary. The southwestern diapir appears as a salt pillow (the D2 diapir). During this step, the absence of pre-kinematic sediments indicates that the diapir initiation occurred early, concurrently with the sedimentation of the Miocene Gachsaran Formation over the salt layer.

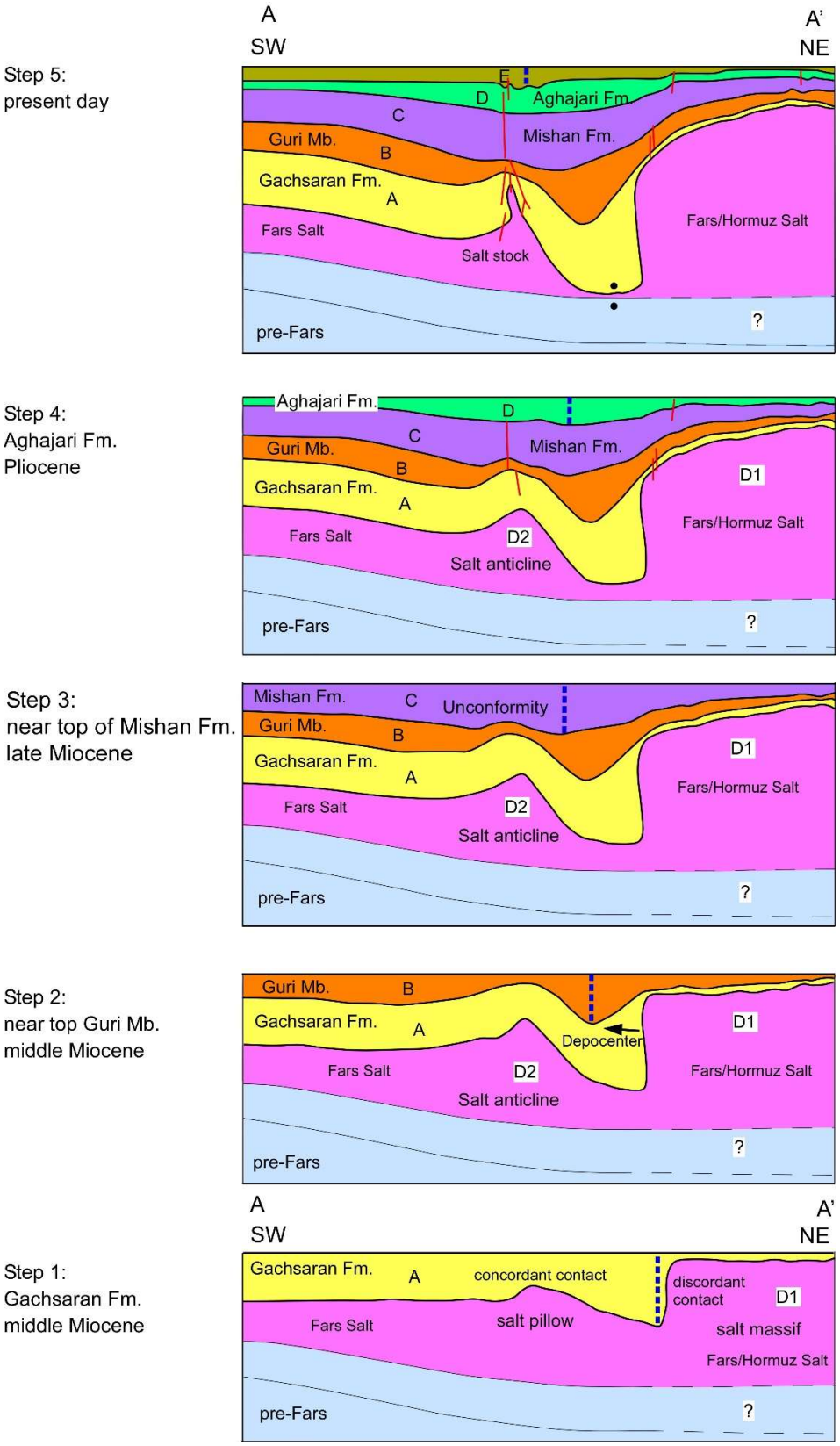

Figure 7. Step-by-step restoration of structural cross-section AA' from the Middle Miocene to the present-day geometry. The cross-section is reconstructed in five steps by flattening the desired horizon at each stage

In the second step, both diapirs experience significant growth, accompanied by substantial subsidence of the minibasin and the initiation of the diapir phase. Concurrently, the depocenter undergoes a sudden migration toward the southwest by 2 km, indicating welding between the bed of the minibasin bottom, adjacent to the D1 diapir, and the top of the pre-salt strata. During this step, salt ascends from the southwestern part, marking the onset of growth for the D2 diapir. The age of sedimentary unit C is assigned to the Middle Miocene, akin to the top of the Guri Member (Fig. 7-2).

Third step: the projection of the anticline in unit B extends out of the sedimentary basin and is then eroded. The eroded section corresponds to the Upper part of the Guri Member. In this step, the depocenter is still migrating, and the minibasin has subsided more. None of the diapirs has reached the seabed in line with the cross-section in this step, and sediments have covered their overhead (Fig. 7-3).

Fourth step: units E and F share the same depocenter location (Fig. 7-4). Faulting is observed above both diapirs and unit D is of the same age of deposition as the lower part of the Aghajari Formation (Pliocene) and the top of the Mishan Formation (Late Miocene) (Fig. 7-5).

Restoration results of BB's cross-section

In the step-by-step and backward-time restoration of the cross-section BB', we observed distinct stages of structural evolution, each contributing to the overall understanding of the geological processes. The chronological steps are outlined below (refer to Fig. 8):

First Step: This phase corresponds to the pre-kinematic sediments, where post-salt sediments are deposited with constant thickness, during the deposition of the Middle Miocene Gachsaran Formation (Fig. 8-1).

Second Step: A salt pillow structure emerges, signifying the beginning of the diapir kinematic stage. The diapir feeds from both southwest and northeast directions, with thicker sediments deposited to the northeast. These sediments are equivalent to the lower part of the Guri Member in the Middle Miocene (Fig. 8-2).

Third Step: Diapir growth intensifies due to rapid sediment deposition and salt feed. The depocenter gradually shifts from the center towards the salt structure, indicating significant salt withdrawal. Welding occurs in the southwestern part of the D3 diapir, while a new salt pillow begins growing in the northeastern part. Sediments from this step correspond to the Middle part of the Guri Member in the Late Miocene (Fig. 8-3).

Fourth Step: New sediments of unit D completely cover the salt and previous deposits. Vertical faulting in the southwestern part intersects units A, B, C, and D. Sediments from this step align with the top of the Guri Member and Mishan Formation in the Late Miocene (Fig. 8-4).

Fifth Step: Sediments of unit E are deposited, and crestal faulting persists during this step. The depocenter of unit E, located near the salt pillow, indicates the growth of salt structure D5. Sediments from this step align with the deposition in the Mishan Formation in the Late Miocene (Fig. 8-5).

Sixth Step: Sediments of unit F are deposited horizontally, with faulting at the top of the salt structure. The depocenter of unit F, adjacent to salt pillow D5, suggests continued salt structure growth. Multiple faults appear at the crest of the salt structure. Sediments from this step are equivalent in age to the Aghajari Formation in Pliocene time (Fig. 8-6).

Discussion

The seismic lines analyzed in this paper broadly align with the stages outlined in Trusheim's model (1957 and 1960) for minibasin evolution. In cross-section AA', our model identifies pre-kinematic sediments, and the salt undergoes rapid growth.

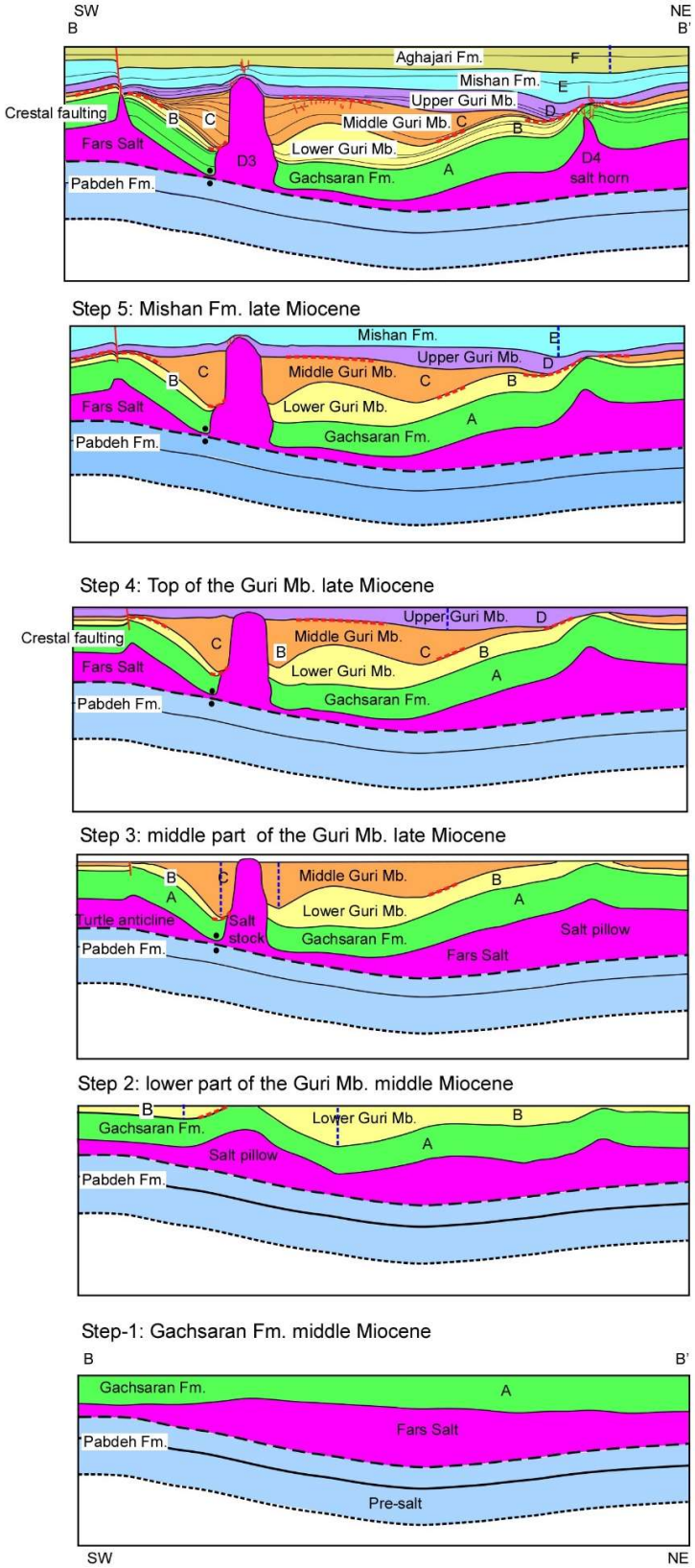

Figure 8. Step-by-step restoration of structural cross-section BB' from the Middle Miocene to the present-day geometry. The cross-section is reconstructed in six steps by flattening the desired horizon at each stage

The pillow stage is notably brief, with the salt structure quickly expanding during the diapir stage, followed by a distinct post-diapir stage. Key differences between our restoration from Trusheim's model include the shorter duration of the pillow stage and the absence of a pre-kinematic stage in seismic line AA'.

Nevertheless, the overall structural geometry, encompassing pre-kinematic stages, the pillow stage, the diapir growth stage, and the post-diapir stage, remains largely consistent with Trusheim's model. The thickness variation observed in surrounding minibasins provides crucial insights into diapir growth, including duration, rate, and orientation. Based on evidence derived from structural geometry interpretation and step-by-step restoration, diapirs D1 and D2 are traced back to their origin in the Fars salt layer.

Recent studies on the salt structures in the southeastern Persian Gulf have generally proposed that Greater Tunb's salt structure results from a combination of deep-seated Hormuz salt and shallow-seated Fars salt (Ezati Asl et al., 2019; Faghih et al., 2019; Hassanpour et al., 2020, 2021; Snidero et al., 2020). During this study, we have not found independent key structures clearly showing the source of salt below the Great Tunb diapir. However, the smaller salt walls surrounding the Great Tunb, are rooted in the Fars Salt layer.

However, it is important to note that the interpretation of Hormuz salt growth beneath Fars salt structures may be subject to geophysical limitations inherent in time seismic data. The primary limitation of time migration in the vicinity of and beneath salt lies in its inability to apply specific velocities to the salt. A well-known issue arising from this limitation is subsalt time pull-up, where seismic waves travel faster through salt than its enclosing sediments, causing mispositioned energy reflections (Hudec & Jackson, 2017). To address this, one alternative pre-salt interpretation approach involves flattening the seismic profile on the pulled-up base of salt. However, this method is effective only to the extent that the base of salt is genuinely planar (Hudec & Jackson, 2017). Additionally, the base of a seismically transparent zone composed of halite typically exhibits near-constant acoustic impedance. Salt sequences entirely made up of halite should, therefore, appear seismically transparent, in contrast to the reflective sediments below supra-salt shale diapirs (Hudec & Jackson, 2017).

Regarding the above-mentioned geophysical limitations, the present-day thickness of Fars salt varies significantly from nearly welded out below grounded minibasins to more than 4500 m in diapirs (Jahani, 2009; Hasanpour et al., 2020). In this study, the restored original depositional thickness of Fars salt is estimated to be 1100–1400 m. This is further supported by the thickness of the Fars salt unit has been about 1200 m in the Ashkan well.

Conclusions

In this study, we present the interpretation and restoration of 2D seismic lines across the southeastern Persian Gulf region to elucidate the evolution of salt diapirs dominantly rooted in the Oligocene to the lower Miocene Fars salt layer. The results reveal a correlation between the growth stages of Fars salt diapirs and flanking minibasins with the classic (Trusheim, 1957, 1960) concept. These stages include: a) the Pre-kinematic stage: Coinciding with the deposition of constant thickness strata of the Gachsaran Formation in the Lower to Middle Miocene, b), concurrent with the base of the Guri Member in the Middle to Late Miocene, c) Passive and rapid growth of diapirs: Recorded by local and very thick depocenters adjacent to salt diapirs, synchronous with Guri Member sedimentation in the Late Miocene, and d) Post-diapirism stage: Involving sediment accumulation above the crestal domain of diapirs during the deposition of the Upper Mishan and Aghajari formations in the Late Miocene to Pliocene.

Acknowledgments

This study is based on the master thesis of the first/corresponding author, performed at the Institute of Advanced Studies in Basic Sciences (IASBS), Zanjan, Iran. The seismic data were kindly provided by the Iranian Offshore (Falat-Ghare) Oil Company. The authors have greatly benefited from scientific discussions with Dr. Ali Chehrazi and Dr. Mahtab Aflaki The authors would like to thank two anonymous reviewers for their constructive comments that improved the quality of the manuscript.

References

Ala, M. A., 1974. Salt diapirism in southern Iran. AAPG Bulletin, 58: 1758-1770.

Alavi, M., 2004. Regional stratigraphy of the Zagros fold-thrust belt of Iran and its proforeland evolution. American Journal of Science, 304: 1-20.

Callot, J. P., Trocmé, V., Letouzey, J., Albouy, E., Jahani, S., Sherkati, S., 2012. Pre-existing salt structures and the folding of the Zagros Mountains. Geological Society, London, Special Publications, 363: 545-561.

Ezati Asl, M. E., Faghih, A., Mukherjee, S., Soleimany, B., 2019. Style and timing of salt movement in the Persian Gulf basin, offshore Iran: Insights from halokinetic sequences adjacent to the Tonb-e-Bozorg salt diapir. Journal of Structural Geology, 122: 116-132.

Faghih, A., Ezati-Asl, M., Mukherjee, S., Soleimany, B., 2019. Characterizing halokinesis and timing of salt movement in the Abu Musa salt diapir, Persian Gulf, offshore Iran. Marine and Petroleum Geology, 105: 338-352.

Fossen, H., 2016. Structural geology. Cambridge University Press.

Ghazban, F., Al-Aasm, I. S., 2007. Hydrocarbon-induced dolomite formation associated with Hormuz salt plug in the Persian Gulf, Iran. In GAC-MAC Annual Meeting. Yellowknife, Abstracts, 32: 31.

Groshong, R. H., Groshong, R. H., 1999. Elements of Map-Scale Structure. 3-D Structural Geology: A Practical Guide to Surface and Subsurface Map Interpretation, 1-32.

Hassanpour, J., Muñoz, J. A., Yassaghi, A., Ferrer, O., Jahani, S., Santolaria, P., SeyedAli, S. M., 2021. Impact of salt layers interaction on the salt flow kinematics and diapirism in the Eastern Persian Gulf, Iran: Constraints from seismic interpretation, sequential restoration, and physical modeling. Tectonophysics, 811: 228887.

Hassanpour, J., Yassaghi, A., Muñoz, J. A., Jahani, S., 2021. Salt tectonics in a double salt-source layer setting (Eastern Persian Gulf, Iran): Insights from the interpretation of seismic profiles and sequential cross-section restoration. Basin Research, 33: 159-185.

Jackson, M. P., Hudec, M. R., 2017. Salt tectonics: Principles and practice. Cambridge University Press.

Jahani, S., Callot, J.-P., Frizon de Lamotte, D., Letouzey, J., Leturmy, P., 2007. The salt diapirs of the eastern Fars province (Zagros, Iran): A brief outline of their past and present. In: Lacombe, O., Lav`e, J., Roure, F., Verg`es, J. (Eds.), Thrust Belts and Foreland Basins. Springer, Berlin, 289–308.

Jahani, S., Callot, J.-P., Letouzey, J., Frizon de Lamotte, D., 2009. The eastern termination of the Zagros Fold-and-Thrust Belt, Iran: Structures, evolution, and relationships between salt plugs, folding, and faulting. Tectonics 28: TC6004.

Kent, P. E., 1979. The emergent Hormuz salt plugs of southern Iran. Journal of petroleum geology, 2: 117-144.

Motiei, H., 1993. Stratigraphy of Zagros. Treatise on the Geology of Iran, 1: 60-151.

Najafi, M., Lajmorak, S., 2020. Contractional salt-tectonic system in the south Dezful embayment, Zagros. Journal of Structural Geology, 141: 104204.

Najafi, M., Beamud, E., Ruh, J., Mouthereau, F., Tahmasbi, A., Bernaola, G., Yassaghi, A., Motamedi, H., Sherkati, S., Goodarzi, M.G.H., Vergés, J., 2021. Pliocene growth of the Dowlatabad syncline in Frontal Fars arc: Folding propagation across the Zagros Fold Belt, Iran. Bulletin, 133: 1381-1403.

Peel, F. J., 2014. How do salt withdrawal minibasins form? Insights from forward modeling, and implications for hydrocarbon migration. Tectonophysics, 630: 222-235.

Pirouz, M., Simpson, G., Chiaradia, M., 2015. Constraint on foreland basin migration in the Zagros Mountain belt using Sr isotope stratigraphy. Basin Research, 27: 714-728.

Snidero, M., Carrera, N., Mencos, J., Butillé, M., Granado, P., Tavani, S., Muñoz, J. A., 2020. Diapir kinematics in a multi-layer salt system from the eastern Persian Gulf. Marine and Petroleum Geology, 117: 104402.

Stewart, S. A., 2018. Hormuz salt distribution and influence on structural style in NE Saudi Arabia. Petroleum Geoscience, 24: 143-158.

Trusheim, F., 1957. Über Halokinese und ihre Bedeutung für die strukturelle Entwicklung Norddeutschlands. Zeitschrift der deutschen geologischen Gesellschaft, 111-158.

Trusheim, F., 1960. Mechanism of salt migration in northern Germany. AAPG Bulletin, 44: 1519-1540.

Vendeville, B. C., 2002. A new interpretation of Trusheim's classic model of salt-diapir growth.